ORIGINAL COMMUNICATION

Imaging respiratory muscle quality and function in Duchenne muscular dystrophy

Alison M. Barnard[1,2] · Donovan J. Lott[1] · Abhinandan Batra[1] · William T. Triplett[1] · Sean C. Forbes[1] · Samuel L. Riehl[1] · Rebecca J. Willcocks[1] · Barbara K. Smith[1] · Krista Vandenborne[1] · Glenn A. Walter[2]

Abstract

Objective Duchenne muscular dystrophy (DMD) is characterized by damage to muscles including the muscles involved in respiration. Dystrophic muscles become weak and infiltrated with fatty tissue, resulting in progressive respiratory impairment. The objective of this study was to assess respiratory muscle quality and function in DMD using magnetic resonance imaging and to determine the relationship to clinical respiratory function.

Methods Individuals with DMD ($n = 36$) and unaffected controls ($n = 12$) participated in this cross sectional magnetic resonance imaging study. Participants underwent dynamic imaging of the thorax to assess diaphragm and chest wall mobility and chemical shift-encoded imaging of the chest and abdomen to determine fatty infiltration of the accessory respiratory muscles. Additionally, clinical pulmonary function measures were obtained.

Results Thoracic cavity area was decreased in individuals with DMD compared to controls during tidal and maximal breathing. Individuals with DMD had reduced chest wall movement in the anterior–posterior direction during maximal inspirations and expirations, but diaphragm descent during maximal inspirations (normalized to height) was only decreased in a subset of individuals with maximal inspiratory pressures less than 60% predicted. Muscle fat fraction was elevated in all three expiratory muscles assessed ($p < 0.001$), and the degree of fatty infiltration correlated with percent predicted maximal expiratory pressures ($r = -0.70$, $p < 0.001$). The intercostal muscles demonstrated minimal visible fatty infiltration; however, this analysis was qualitative and resolution limited.

Interpretation This magnetic resonance imaging investigation of diaphragm movement, chest wall movement, and accessory respiratory muscle fatty infiltration provides new insights into the relationship between disease progression and clinical respiratory function.

Keywords MRI · Diaphragm · Pulmonary · Neuromuscular disease · Dixon imaging

Introduction

Duchenne muscular dystrophy (DMD) is the most common pediatric muscular dystrophy, affecting approximately 1 in 5000–6300 males [1, 2]. DMD is a life-limiting muscle degenerative disorder caused by mutations in the dystrophin gene [3]. In DMD, skeletal muscles, including the muscles of respiration, are fragile undergoing damage, inflammation, and ultimately replacement by fibrofatty tissue, resulting in progressive weakness [4, 5]. Respiratory insufficiency is ubiquitous in later stages of DMD, and airway clearance techniques and respiratory support are eventually necessary to maintain adequate ventilation [6]. Respiratory complications are a major cause of morbidity and mortality [7].

Clinically, respiratory health is assessed using measures such as spirometry and maximal inspiratory and expiratory pressures, and the natural progression of these measures is well characterized in DMD [8]. Expiratory function, crucial for coughing and airway clearance, is compromised first, with signs of decreased maximal expiratory pressure (MEP) as early as the first decade of life [9, 10]. Inspiratory function is initially maintained, with maximal inspiratory pressure consistently higher than MEP [11]. Forced vital

✉ Glenn A. Walter
  glennw@ufl.edu

1 Department of Physical Therapy, University of Florida, Gainesville, FL, USA

2 Department of Physiology and Functional Genomics, University of Florida, Gainesville, FL, USA

capacity (FVC), which reflects both inspiratory and expiratory capacity, initially improves due to growth, peaks in the mid-teenage years, then progressively declines [11, 12]. Percent predicted FVC (%pFVC) typically declines steadily, beginning as early as 6–8 years old [11, 12].

Despite the utility of clinical assessments of respiratory health, these measures are non-specific, have poor sensitivity, and provide limited insight into the pathophysiology of the respiratory muscles themselves. Specific knowledge of disease progression in the diaphragm, the primary muscle of inspiration, and the accessory respiratory muscles (intercostals and abdominals) is incomplete, as is the relationship between muscle pathology and clinical respiratory function. Magnetic resonance imaging (MRI) is a noninvasive tool that can quantify different aspects of muscle health in DMD [13–16]. Measures of muscle fatty infiltration are MR biomarkers of disease progression, and the degree of fatty infiltration has been shown to correlate well with clinical tests of limb muscle function [17–20]. At present, there are no quantitative MR studies of accessory respiratory muscle fatty infiltration in DMD. Diaphragm size precludes the quantification of structural MR parameters with current clinical technology [21, 22]; however, dynamic MRI can capture diaphragm and chest wall motion during breathing [23]. The use of dynamic MRI to assess respiratory motion has been piloted for DMD in two previous studies [24, 25]. Although limited by small sample sizes, both studies show the potential value of dynamic MRI in expanding the understanding of diaphragm function and chest wall mechanics, as well as how these factors contribute to respiratory status.

It is not well understood how replacement of muscle by noncontractile tissue, diaphragm weakness, and altered chest mobility contributes to changes in clinical respiratory function. Therefore, this study assessed these processes and their relationship to respiratory impairment in DMD using MRI in a diverse cohort of ambulatory and nonambulatory participants. We assessed disease progression of the accessory respiratory muscles using chemical shift-encoded (CSE) MRI to quantify muscle fatty infiltration, and we evaluated diaphragm and chest wall motion during tidal and maximal breathing using dynamic MRI.

Methods

Participant enrollment and study design

Participants with DMD and unaffected controls were enrolled in this observational natural history study. Each study visit included an MRI exam followed by clinical pulmonary function testing. To be included in the study, individuals with DMD were required to be at least 5 but less than 19 years old at enrollment, have a confirmed diagnosis of DMD, be able to lie flat in the magnet for the duration of the exam, and not have any comorbid respiratory complications such as uncontrolled asthma. Control participants were included if they had no history of respiratory disease and no conditions affecting the musculoskeletal system. The study was approved by the Institutional Review Board at the University of Florida. Parents of participants less than 18 years old provided written informed consent, while the child provided written assent. Participants who were 18 gave written informed consent themselves.

MRI acquisition and analysis

The MR exam consisted of chemical shift-encoded (CSE) MRI (also known as Dixon imaging) of the chest and abdominal musculature as well as dynamic MRI (a single slice imaged repeatedly over time) while participants performed breathing maneuvers as described below. All MR data were acquired using a Philips 3 T Achieva MRI (Philips, Amsterdam, Netherlands) with a 32-channel cardiac coil. For imaging of the chest, participants were positioned in supine with the coil centered over the heart, ensuring coil coverage over the entirety of the lungs. CSE imaging of the chest utilized a four-lead VCG (VectorCardioGraphy) signal and a respiratory pillow to gate image acquisition. This allowed for free-breathing imaging. For abdominal imaging, the coil was centered over the umbilicus, and gating was not required. Participants were able to watch a movie or listen to music during the scan session (approximately 40–50 min in length).

Dynamic imaging

Dynamic MRI was performed to assess chest wall and diaphragm excursion during tidal breathing, maximal inspirations, and maximal expirations. The respiratory maneuvers were practiced on the MRI table prior to image acquisition to ensure participant comprehension, and an assistant remained inside the MRI room for additional instruction if needed. Single-slice sagittal plane images were acquired by slicing through the apex of the right lung and bisecting the lung area in the coronal plane. Single-slice coronal plane images were acquired by slicing through both lung apexes and bisecting the lung area in the sagittal plane. Slice plane position was identical for both tidal and maximal breathing. A turbo field echo sequence (TR $= 3.1$ ms, TE $= 1.65$ ms, flip angle $= 15°$, slice thickness $= 8$ mm, resolution $= 1.8 \times 1.8$ mm^2, acceleration factor $= 2.5$) was used to acquire 150 frames at a rate of approximately 5 frames/sec for both tidal and maximal breathing.

Images were exported as DICOMs, and the different frames from the dynamic MRI scans were analyzed to assess thoracic cavity size parameters and diaphragm/chest

Fig. 1 Representative dynamic MRIs, analysis parameters, and ▶ chemical shift-encoded MRIs. Dynamic imaging was performed in the sagittal plane (**a**, **b**) and coronal plane (**c**, **d**) (control = 12.8 years old, individual with DMD = 12.3 years old). Lung size measurements included sagittal plane lung area, anterior–posterior (AP) chest diameter measured at the level of the top of the diaphragm, craniocaudal (CC) length measured from the apex of the lung to the AP chest diameter line, and left–right (LR) chest width measured at the level of the top of the right diaphragm dome. **e** Diaphragm movement after a maximal inspiration or expiration was quantified in the sagittal image, and chest movement was quantified in the sagittal and **f** coronal images. CSE MRIs were acquired at the chest and abdomen. They were reconstructed to produce fat (**g**) and water (**h**) images, and FF was quantified for the abdominal muscles indicated in the CSE out-of-phase image in **i**. *FRC* functional residual capacity, *MAX* maximal inspiration, *RA* rectus abdominis, *EO* external oblique, *IO* internal oblique, *PS* paraspinals, *CSE* chemical shift-encoded, *FF* fat fraction

displacement parameters using OsiriX MD (v.9.5.2), an FDA 510(k)-cleared DICOM viewer. For size parameters, the sagittal plane dynamic images were analyzed to assess right lung area, anterior–posterior (AP) chest diameter, and craniocaudal (CC) length at end tidal expiration (corresponding to functional residual capacity), end tidal inspiration, maximal inspiration, and maximal expiration (Fig. 1a, b). End tidal inspiration and end tidal expiration were determined from the most inferior and superior positions, respectively, of the diaphragm during the respiratory cycle. Up to ten tidal breaths were analyzed and size measures were averaged over the breaths. The quiet and maximal breathing coronal images were also analyzed to assess left–right (LR) chest diameter (Fig. 1c, d).

To assess displacement parameters, the differences in diaphragm and chest wall position during tidal and maximal breathing were determined. Sagittal plane diaphragm descent, sagittal plane chest expansion, and coronal plane chest expansion were determined for maximal inspirations by assessing displacement from functional residual capacity (FRC) position (determined during quiet breathing) to maximal inspiration position. Displacement was averaged over the length of the chest wall or diaphragm to give a mean displacement value (Fig. 1e, f). Average diaphragm elevation and chest wall depression were also calculated at maximal expiration in the sagittal plane, again with FRC position as a starting reference. Size and displacement parameters that could be affected by participant height are reported both as absolute values and normalized values (absolute value divided by participant height).

Chemical shift-encoded imaging

Chemical shift-encoded MRI was performed to quantitatively assess fatty infiltration of the accessory respiratory muscles (intercostals, rectus abdominis, external oblique, and internal oblique) and other muscles of the chest and trunk. Single-slice images of the chest were acquired in the

DYNAMIC IMAGING

CHEMICAL SHIFT-ENCODED MRI
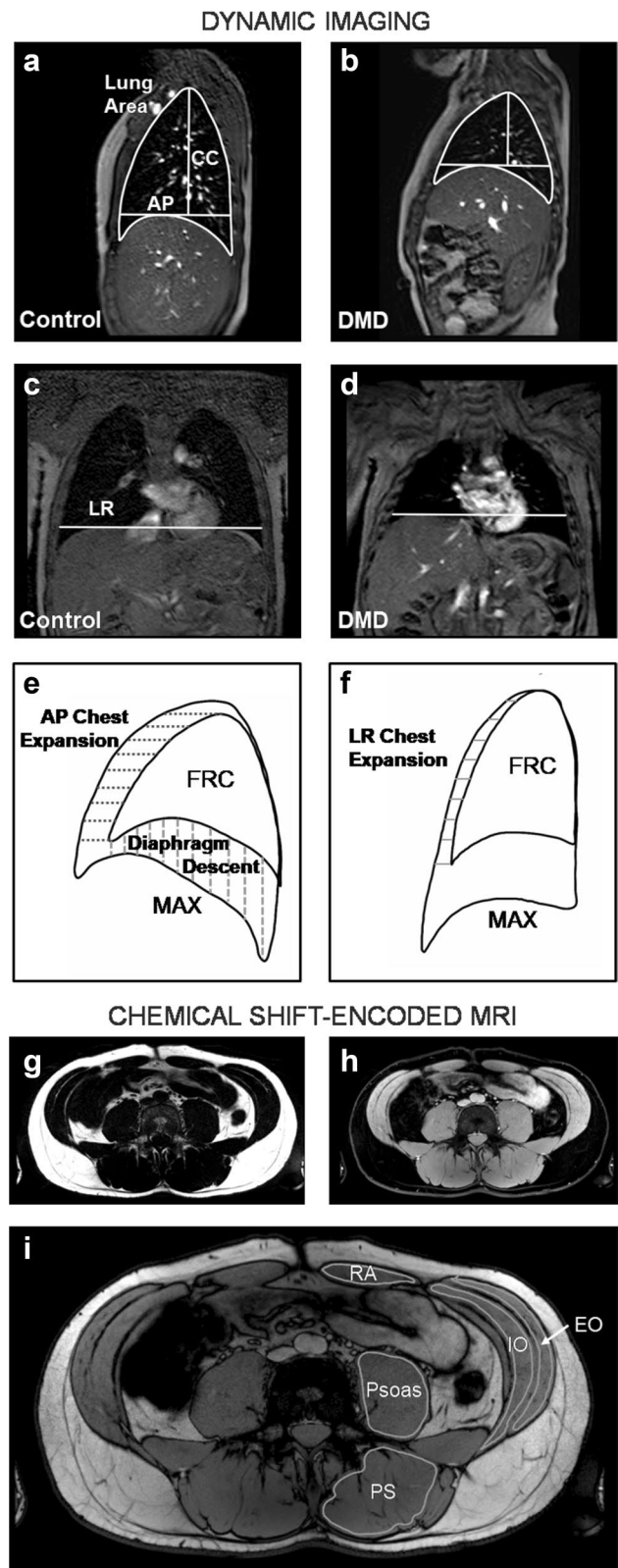
coronal plane, bisecting the rib cage at its widest point, and in the axial plane just below the aortic arch and at the top of the liver. Additionally, a single-slice axial image of the

abdomen was acquired at the level of the umbilicus (approximately at the base of the L4 vertebra). If susceptibility artifacts from intestinal gas obscured musculature, a second axial abdominal image was acquired approximately 2 cm lower. A three-point mDIXON protocol (Philips R5.3) was used with $TR = 10$ ms (gated); $TE = 5.4$, 6.4, and 7.4 ms; slice thickness $= 6$ mm, resolution $= 0.6$ mm $\times$ 0.6 mm, NSA $= 6$, and flip angle $= 10°$. A SENSE acceleration factor of two was used to reduce scan time for the gated axial and coronal chest images.

Chemical shift-encoded magnitude images were reconstructed online to produce water and fat images using the pre-calibrated seven-peak lipid model provided by the Philips 5.3.0 software, and images were exported as DICOMs (Fig. 1g–i). Colorized fat–water fusion images were created using OsiriX MD (v.9.5.2) to visualize muscle fatty replacement in the chest and abdominal muscles. FF was quantified in the abdominal images for the following muscles: the rectus abdominis (RA), external oblique (EO), internal oblique (IO), psoas, and paraspinals (PS) (Fig. 1i). Using OsiriX software, regions of interest were drawn on the reconstructed fat and water images just inside the borders of the muscle. Muscle FF was quantified using the formula FF = fat signal/(fat + water signal). Since fatty infiltration was visually symmetric, only the muscles on the left side of the body were analyzed unless there were air artifacts or unclear muscle borders; in those cases, the muscles on the right side of the body were analyzed. Muscle FF was determined by two independent analyzers (analyzer 1: not blinded and analyzer 2: blinded to participant name and disease severity) for all participants with DMD to determine inter-analyzer reliability. Intraclass correlation coefficient (ICC) and coefficient of variation (CV) were as follows: EO: ICC = 0.99, CV = 5.3%; IO: ICC = 0.99, CV = 5.9%; Psoas: ICC = 0.99, CV = 5.0%; PS: ICC = 0.99, CV = 2.8%; RA: ICC = 0.97, CV = 7.4%.

Pulmonary function testing

Pulmonary function measures included forced vital capacity (FVC), cough peak flow (CPF), maximal inspiratory pressure (MIP), and maximal expiratory pressure (MEP). These are the primary measures recommended for clinical assessment of respiratory function in DMD [8]. Spirometry was performed using a Carefusion Microlab portable spirometer (San Diego, CA). Participants performed an FVC maneuver in sitting and supine, and the volume in liters was recorded. The decrease in FVC from sitting to supine positions was statistically significant in DMD but not clinically meaningful (mean difference -0.07 ± 0.16L); therefore, FVC in sitting was used for all analyses. The percent predicted FVC (%pFVC) was calculated using the recommended reference equations for individuals with DMD, taking into account age, height, and ethnicity

[26]. For nonambulatory participants, height was calculated in supine by summing segmental measurements (head to greater trochanter, greater trochanter to lateral epicondyle of the knee, and lateral epicondyle of the knee to the distal calcaneus). CPF was assessed during maximal coughs performed after a large inspiration, and results were recorded in L/s.

MIP and MEP tests were performed in a sitting position using a Carefusion MicroRPM device (San Diego, CA). For MIP, participants emptied their lungs to residual capacity and then inspired as forcefully as possible, and for MEP, participants inspired to total lung capacity and then exhaled as forcefully as possible with gentle manual pressure at the cheeks. The highest pressure generated at the mouth was recorded in cm H_2O, and percent predicted values were calculated using reference equations [27]. For all tests, participants wore nose clips, and strong encouragement was provided to elicit maximal effort. A minimum of three and maximum of six efforts were performed, aiming for three valid results within 10% of each other. The highest value was used for analysis.

Lower extremity muscle fat fraction

A large subset of the individuals with DMD ($n = 32$) in this study was co-enrolled in the ImagingDMD natural history study (NCT01484678; imagingdmd.org), and these individuals underwent lower extremity MR assessment during the same study visit. Vastus lateralis and soleus muscle FF values, determined using single-voxel proton magnetic resonance spectroscopy (MRS), were available from the ImagingDMD data set to compare to respiratory imaging measures. Methods for acquisition and analysis of MRS FF have been previously described in detail [28].

Statistical analysis

Analyses were performed using GraphPad Prism version 7.03 (La Jolla, CA). Differences between control participants and individuals with DMD were assessed using independent t tests with Welch's correction as needed, and differences between control participants and subgroups of participants with DMD were assessed using ANOVA with Tukey's post hoc testing. For pairwise comparisons between muscle groups for the same participants, data were analyzed using paired t tests. All correlation coefficients were determined using Pearson's correlation test. Significance was set at $\alpha < 0.05$.

Results

A total of 36 individuals with DMD (7.3–18.8 years old) and 12 unaffected controls (6.3–18.3 years old) participated in the study (Table 1). Of the individuals with DMD, 25 were

ambulatory, and 32 were on corticosteroids. Age, weight, and BMI were not significantly different between the control and DMD groups; however, the control participants were taller ($p = 0.002$). Respiratory function was significantly higher in the control group than in individuals with DMD for all measures collected. Respiratory function in the DMD cohort ranged from normal to severely impaired, and results are detailed in Table 1. Seven participants with DMD reported regularly using a cough assist device for airway clearance, and three reported use only when sick or congested. One individual reported routinely using BiPAP at night as well as daytime open circuit mouthpiece ventilation as needed.

Dynamic imaging

Sagittal plane lung area was significantly smaller in participants with DMD compared to controls at FRC, end tidal inspiration, maximal inspiration, and maximal expiration (Table 2). Participants with DMD also had significantly shorter craniocaudal (CC) thoracic cavity lengths. Since unaffected controls were taller than the participants with DMD, lung area and CC lengths were normalized to height, and significant differences remained even after normalization. Left–right (LR) chest widths and anterior–posterior (AP) chest diameters tended to be larger in controls, but differences were not significant. The difference between lung area at maximal inspiration and maximal expiration was positively correlated with FVC ($r = 0.93$, $p < 0.001$).

When maximally inspiring, controls increased their sagittal plane lung area more than individuals with DMD ($p = 0.003$), even when normalizing to height ($p < 0.001$) (Fig. 2). Absolute diaphragm descent was larger in controls than in DMD during maximal inspirations; however, when normalized to height, these differences were no longer significant. MIP and %pMIP were correlated to both absolute diaphragm descent ($r = 0.57$, $p < 0.001$ and $r = 0.42$, $p = 0.017$) and diaphragm descent normalized to height ($r = 0.56$, $p = 0.001$ and $r = 0.53$, $p = 0.002$). Individuals with DMD were classified as having minimally

Table 1 Participant characteristics

	Controls, $N = 12$	DMD, $N = 36$	p value
Age (years)	13.9 (6.3–18.3)	12.6 (7.3–18.8)	ns ($p = 0.259$)
Height (cm)	161 (117–191)	132 (117–160)	*$p = 0.002$
Weight (kg)	55.4 (21.4–90.3)	40.8 (24.0–71.2)	ns ($p = 0.054$)
BMI	20.3 (15.9–28.2)	23.0 (16.3–36.6)	ns ($p = 0.156$)
FVC (L)	4.08 (1.44–5.91)	1.89 (0.79–3.17)	*$p < 0.001$
%pFVC	103% (96–114%)	86% (39–134%)	*$p < 0.001$
CPF (L/s)	372.8 (147.6–551.4)	223.9 (132.6–423.0)	*$p = 0.003$
MIP (cmH$_2$O)	103 (55–152)	64 (24–103)	*$p < 0.001$
%pMIP	120% (91–154%)	85% (31–155%)	*$p < 0.001$
MEP (cmH$_2$O)	105 (74–158)	64 (26–105)	*$p < 0.001$
%pMEP	96% (51–141%)	62% (25–140%)	*$p < 0.001$

Data are reported as mean (range). *Indicates a statistically significant difference between the control and DMD groups. (*ns* not significant)

Table 2 Lung size and dimensions

	FRC	End tidal inspiration	Maximal inspiration	Maximal expiration
Lung area (cm^2)				
Controls	150.8 ± 50.1	172.2 ± 50.8	284.4 ± 88.5	138.0 ± 38.9
DMD	91.1 ± 20.5*	106.7 ± 21.8*	170.9 ± 25.1*	79.3 ± 19.1*
CC length (CM)				
Controls	14.5 ± 3.2	15.9 ± 3.1	19.6 ± 4.1	14.4 ± 2.9
DMD	9.5 ± 1.8*	10.4 ± 1.9*	12.7 ± 1.9*	8.8 ± 1.8*
AP length (cm)				
Controls	12.7 ± 2.0	13.1 ± 2.0	15.3 ± 2.1	12.2 ± 1.9
DMD	12.1 ± 1.3	12.5 ± 1.3	14.5 ± 1.2	11.3 ± 1.2
LR length (cm)				
Controls	22.8 ± 3.4	23.1 ± 3.2	25.7 ± 3.7	22.2 ± 3.7
DMD	20.7 ± 1.6	21.4 ± 1.6	24.2 ± 1.8	20.3 ± 1.7
Lung area/Ht (cm^2/cm)				
Controls	0.9 ± 0.2	1.1 ± 0.2	1.7 ± 0.3	0.8 ± 0.2
DMD	0.7 ± 0.1*	0.8 ± 0.1*	1.3 ± 0.1*	0.6 ± 0.1*
CC length/Ht (cm/m)				
Controls	9.0 ± 0.9	9.8 ± 0.9	12.0 ± 1.0	8.6 ± 1.0
DMD	7.1 ± 1.2*	7.8 ± 1.2*	9.6 ± 1.4*	6.6 ± 1.1*

Data are expressed as mean ± SD. *Indicates a statistically significant difference between the control and DMD groups ($p < 0.05$). (*FRC* functional residual capacity, *CC* craniocaudal, *AP* anterior–posterior, *LR* left–right)
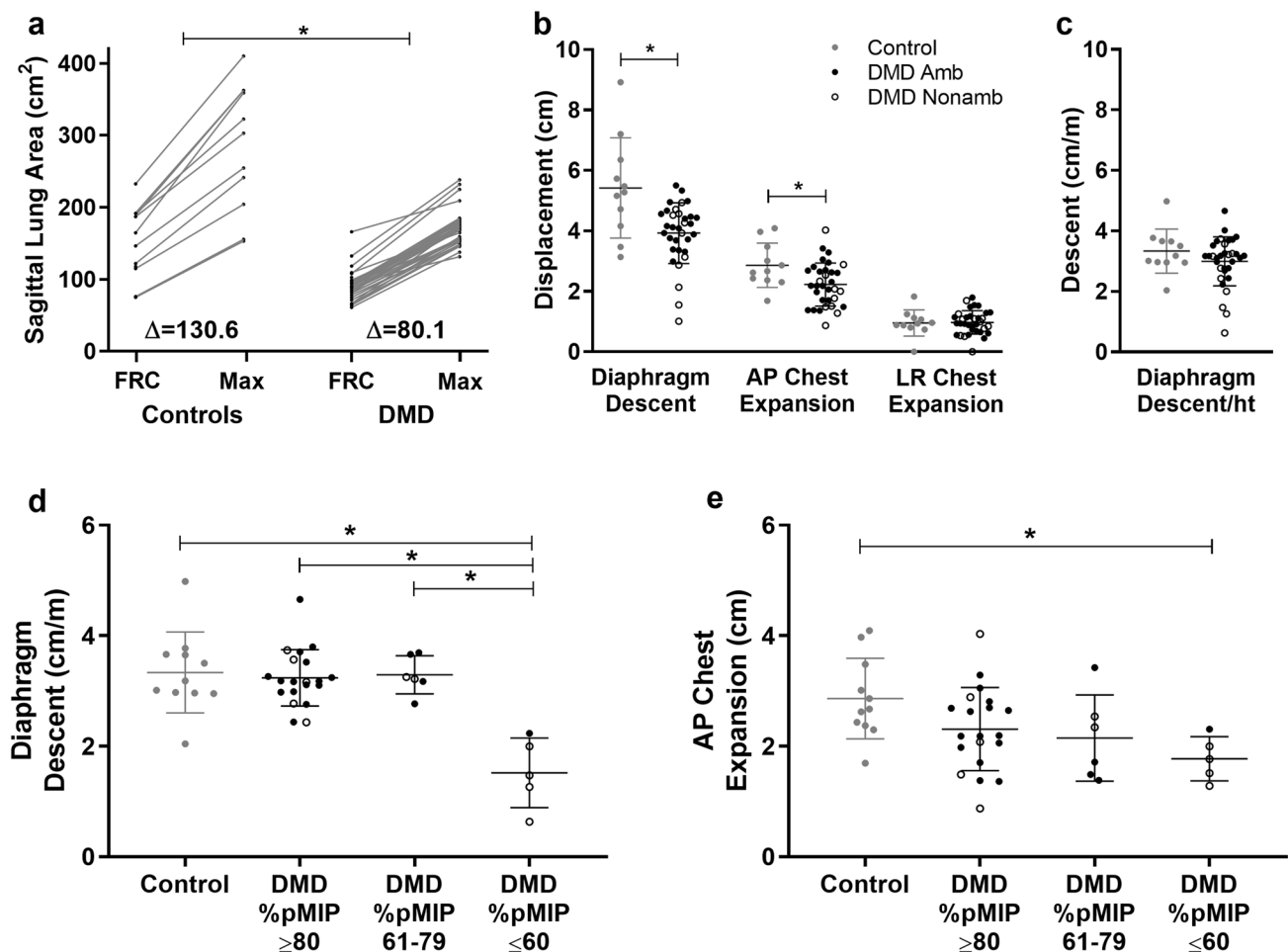
Fig. 2 Lung area increase, diaphragm descent, and chest expansion during a maximal inspiration. **a** Unaffected controls had larger sagittal plane lung areas at functional residual capacity (FRC) and at maximal inspiration (max) than participants with DMD, and they also had larger increases in lung area during maximal inspirations ($p = 0.003$). **b** Additionally, controls (gray circles) had larger diaphragm descent ($p = 0.015$) and anterior–posterior (AP) chest expansion ($p = 0.015$) compared to individuals with DMD (ambulatory = closed black circles, nonambulatory = open black circles), but there was no difference in left–right (LR) chest expansion. **c** When diaphragm descent was normalized to height, differences were no longer significant between groups. **d** However, the subgroup of participants with DMD with percent predicted MIP (%pMIP) ≤ 60 had significantly reduced diaphragm descent normalized to height and **e** AP chest expansion compared to controls. *$p < 0.05$

affected MIP ($\geq 80\%$ predicted, $n = 23$), moderately affected MIP (> 60 to $< 80\%$ predicted, $n = 6$), or severely affected MIP ($\leq 60\%$ predicted, $n = 5$). Individuals with MIPs $\leq 60\%$ had significantly reduced normalized diaphragm descent compared to all other participants. No control had diaphragm descent ≤ 2.0 cm/m, whereas four out of five individuals with %pMIPs $\leq 60\%$ had diaphragm descent ≤ 2.0 cm/m. When maximally inspiring, AP chest expansion was reduced in DMD compared to controls ($p = 0.015$), and separating the DMD cohort into groups by %pMIP revealed that chest expansion limitations were most pronounced in the %pMIP $\leq 60\%$ group. There were no differences in chest expansion in the LR direction between groups.

During maximal expirations, controls had larger decreases in sagittal plane lung area from FRC to minimum area than individuals with DMD ($p < 0.001$) (Fig. 3). Individuals with DMD had reduced diaphragm elevation in the sagittal plane ($p < 0.001$), and interestingly 13 out of 30 participants with valid exhales had either no diaphragm elevation or some degree of diaphragm descent rather than elevation. There was also significantly reduced chest depression in the AP direction in the DMD group ($p = 0.0105$). Neither diaphragm elevation nor chest wall depression during a maximal expiration was correlated to clinical measures of pulmonary function or expiratory muscle FF.
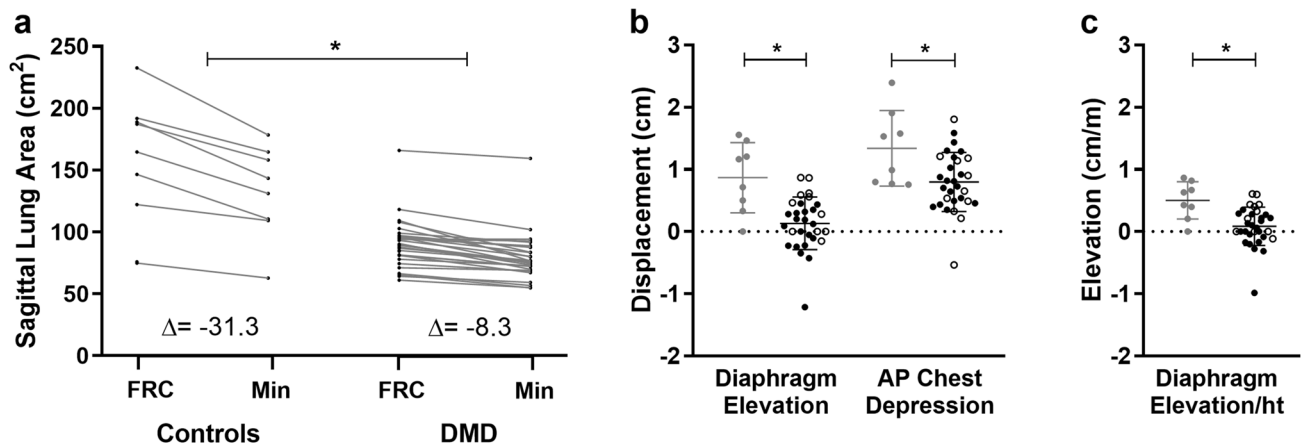
Fig. 3 Lung area decrease, diaphragm elevation, and chest depression during a maximal expiration. **a** In addition to having larger sagittal plane lung areas after a maximal expiration, control participants had larger absolute decreases in lung area during maximal expirations (min) compared to participants with DMD ($p < 0.001$). **b** Diaphragm elevation and anterior–posterior (AP) chest depression were also significantly reduced in participants with DMD (ambulatory = closed black circles, nonambulatory = open black circles) compared to controls (gray circles). Several participants with DMD had paradoxical diaphragm movement during maximal expirations, and one participant (not the same outlier for diaphragm movement) had paradoxical chest movement. These cases correspond with the negative values in (**b**). **c** Diaphragm elevation was significantly reduced in DMD compared to controls even after normalization to height (ht). *$p < 0.05$

Chemical shift-encoded MRI

Axial fat–water fusion images, created from CSE scans, of the abdomen of control participants had little to no visible fatty infiltration of the expiratory respiratory muscles, and quantification of FF revealed that control participants had an average muscle FF of 0.09 ± 0.04 (Fig. 4a, b). In DMD, FF ranged from minimal levels to nearly complete replacement of muscle by fat (0.06–0.94), and as a group, FF was significantly elevated above control levels for each of the expiratory muscles ($p < 0.001$ for all group comparisons). In this cohort of DMD participants, the internal oblique was consistently more infiltrated than the external oblique (mean FF = 0.49 vs 0.41, $p < 0.001$), and the external oblique was consistently more infiltrated than the RA (mean FF = 0.41 vs 0.33, $p < 0.001$). Expiratory muscle FF correlated positively with age for all three muscles, but the strongest correlation was found between age and IO FF ($r = 0.67$, $p < 0.001$; Fig. 4c). There was a negative linear correlation between expiratory muscle FF and %pMEP in DMD with IO FF correlating most strongly ($r = -0.70$, $p < 0.001$) (Fig. 4d). In a linear regression, IO FF explained an additional 10% of the variance in %pMEP beyond that explained by age alone. Cough peak flow was not significantly correlated to expiratory muscle FF.

Fat–water fusion images of the chest revealed little to no observable fat in the chest and upper trunk muscles of control participants. However, in DMD, fatty infiltration of the chest and upper trunk muscles ranged from minimal to extensive (Fig. 5). Fatty infiltration was visible in the pectoralis, scapular, serratus anterior, latissimus dorsi, and thoracic paraspinal muscles. Strikingly, the intercostals, which are important accessory respiratory muscles, appeared to have less fatty infiltration; however, further study is needed to confirm this finding in these small muscles (Fig. 5).

Respiratory MR measures, LE MR measures and ambulatory status

To evaluate the disease progression of the respiratory muscles in the context of other skeletal muscles, expiratory muscle FF was compared to MRS-derived FF of two key lower extremity muscles, the VL and SOL muscles, from 32 participants co-enrolled in ImagingDMD (NCT01484678). Additionally, the FFs of two other lower trunk muscles visible on the abdominal MRIs (paraspinals—spinal extensors and psoas—hip flexor) were quantified for comparison. Figure 6a compares the FF of the seven different muscles with the paraspinals being globally most affected (mean FF = 0.53). The degree of disease progression in the expiratory muscles was related to overall disease progression in the leg and trunk muscles. The amount of fatty infiltration of the IO was most similar to that of the paraspinals, and the amount of EO fatty infiltration was most similar to that of the VL muscle.

Loss of ambulation is often a clinical milestone indicating a need to begin monitoring pulmonary status more closely. In this cohort, nonambulatory individuals had significantly lower %pFVC (91.4 ± 3.4 vs 75.7 ± 7.8%, $p = 0.038$), lower %pMIP (93 ± 5 vs 70 ± 7%, $p = 0.015$), and lower %pMEP (71 ± 6 vs 43 ± 5%, $p = 0.001$) than ambulatory participants. Additionally, nonambulatory individuals had significantly
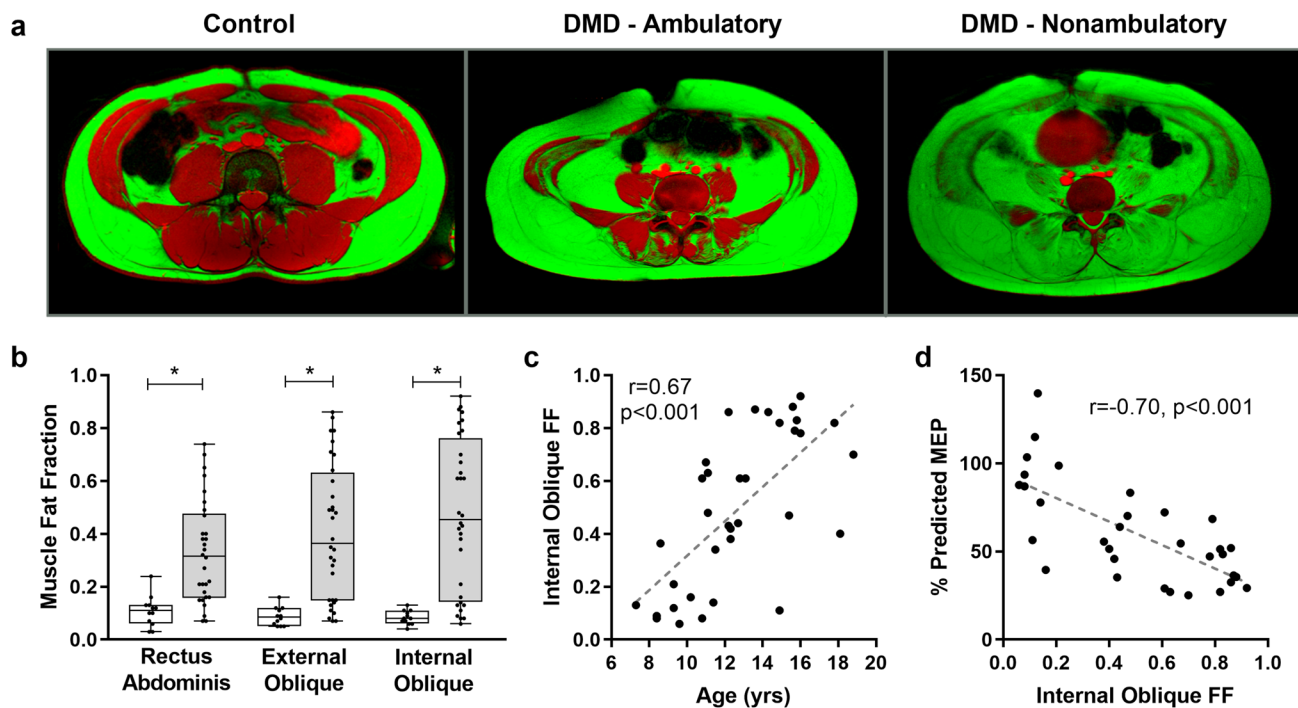
Fig. 4 Expiratory muscle fat fraction. **a** Fat (green) and water (red) fusion images of the abdominal and expiratory muscles of a 16 year old unaffected control, an ambulatory 13 year old with DMD, and a nonambulatory 16 year old with DMD. Significant fatty infiltration of the expiratory muscles is visible in the individuals with DMD, and early involvement of the internal oblique was consistently seen even in ambulatory participants. **b** Fat fraction (FF) was elevated in DMD compared to controls for each expiratory muscle analyzed. The rectus abdominis was, on average, the least affected expiratory muscle, while the internal oblique was the most affected. **c** Internal oblique FF increased with increasing age ($r = 0.67$, $p < 0.001$). **d** Internal oblique FF was significantly correlated with percent predicted maximal expiratory pressure (%pMEP) ($r = -0.70$, $p < 0.001$). *$p < 0.05$

smaller increases in sagittal plane lung area/height and reduced diaphragm descent/height during maximal inspirations (Fig. 6b). The four individuals with normalized diaphragm descent ≤ 2.0 cm/m during maximal inspirations had advanced disease progression. All were nonambulatory and had a mean VL FF = 0.76, SOL FF = 0.62, FVC = 1.46L, %pFVC = 51%, %pMIP = 45%, and %pMEP = 32%. Finally, nonambulatory individuals had higher expiratory muscle FFs than ambulatory individuals (Fig. 6c); however, many ambulatory participants already had expiratory muscle FFs > 0.5.

Discussion

MRI is an established and powerful tool to noninvasively assess muscle health in neuromuscular disorders; however, its use in DMD has largely been focused on cardiac and limb muscles. Respiratory impairment contributes significantly to morbidity, mortality, and decreased quality of life in DMD [29], yet quantitative MRI has only been utilized in a limited manner to investigate respiratory involvement [24, 25]. MRI techniques allow for the ability to noninvasively assess

diaphragm function in vivo, to assess thoracic cage dynamics during breathing, and to evaluate disease progression in individual respiratory muscles. This study represents the first quantitative MRI investigation of accessory respiratory muscle composition and the largest MRI study of chest and diaphragm dynamics in DMD across a range of ages and abilities. Key findings from the study include: (1) reduced AP chest wall mobility and impaired diaphragm movement during maximal breathing in DMD; (2) early fatty infiltration of the muscles of forced expiration, particularly the internal oblique; and (3) less severe fatty infiltration of the intercostals compared to surrounding chest muscles.

A recent review of respiratory muscle imaging in neuromuscular disease highlighted the potential for breathhold and dynamic MRI to provide insights into diaphragm and respiratory function [30]. However, in DMD, only two dynamic imaging studies in small cohorts have been published by Mankodi et al. ($n = 11$ ambulatory DMD; $n = 15$ controls) and by Bishop et al. ($n = 13$ nonambulatory DMD; $n = 10$ controls) [24, 25]. Both studies performed dynamic imaging in the sagittal plane during FVC maneuvers. The present study builds upon their dynamic imaging findings by examining inspiratory and expiratory efforts separately
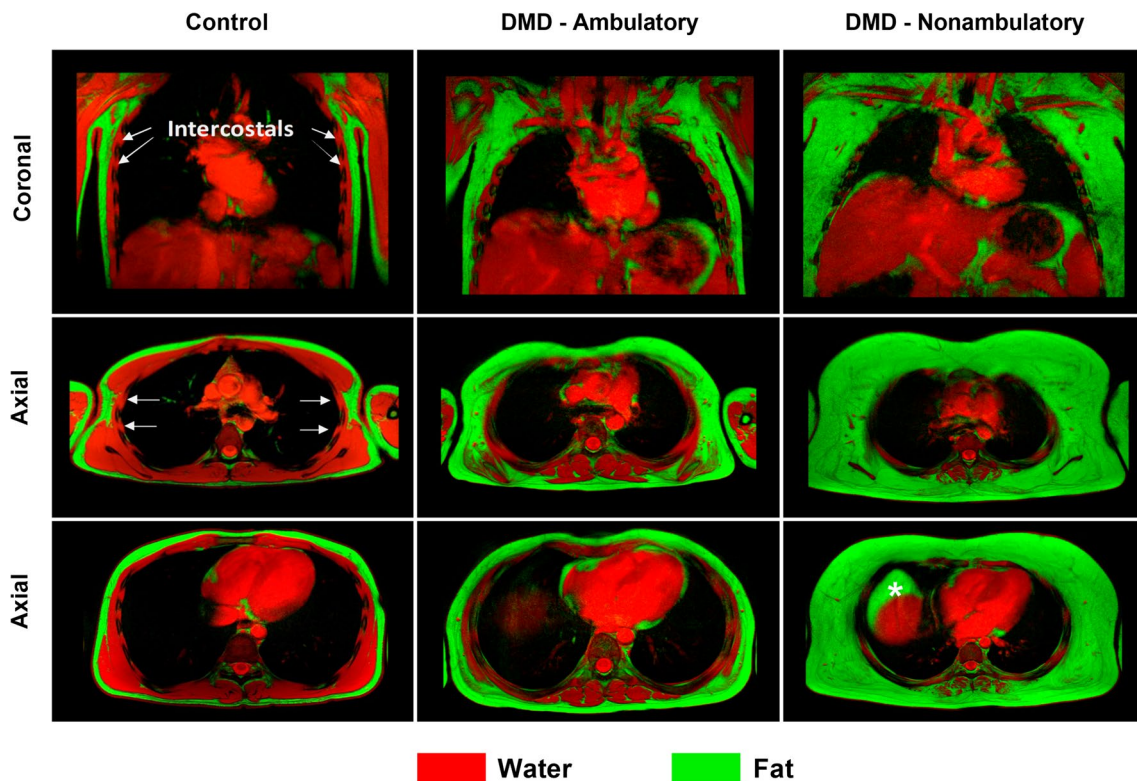
Control   **DMD - Ambulatory**   **DMD - Nonambulatory**

Coronal Axial Axial

Intercostals

■ Water   ■ Fat

Fig. 5 Fat–water fusion images of the chest. Fat (green) and water (red) images of the chest were acquired in the coronal and axial planes and overlaid to produce fusion images for a 17 year old unaffected control, an ambulatory 12 year old with DMD, and a nonambulatory 12 year old with DMD. In the individuals with DMD, fatty infiltration is visible in the muscles of the chest. The serratus anterior, which is visible overlying the ribs in the coronal image of the control participant is completely infiltrated with fat in the nonambulatory individual with DMD. However, the intercostal muscles, which are accessory respiratory muscles located between the ribs and beneath the serratus anterior, demonstrate less involvement than the other chest muscles. (Note: In the nonambulatory participant, a pocket of fatty tissue, denoted by an asterisk, is visible anterior to the liver and represents true fat rather than a fat–water switching artifact)

in a broader cohort and adds novel information about fatty infiltration of the expiratory and chest wall muscles.

Participants with DMD in this study had smaller thoracic cavities than controls, and these findings are consistent with those of Mankodi et al. and Bishop et al. Since stature is one of the major determinants of lung volume [26], it is likely that the shorter stature resulting from long-term steroid treatment in the majority of participants is a contributing factor to the smaller lung cross sectional areas and smaller rib cage dimensions in DMD [31]. No precedent has been developed for normalizing respiratory MRI measures in individuals of differing height. If differences in height are not accounted for, it is difficult to determine whether differences in lung cross sectional area, diaphragm movement, and chest wall movement result from true muscle weakness and respiratory dysfunction or are simply a result of having smaller thoracic cavities and shorter stature. In this study, results of both absolute values and values normalized to height have been included when appropriate, and future studies should keep these thoracic cavity size differences in mind when assessing respiratory dynamics.

Results of dynamic MRI during maximal inspirations and expirations demonstrate impairments in both diaphragm and chest wall movement. During maximal inspirations, decreased diaphragm descent was correlated with reduced MIPs, and a subgroup of individuals with MIP ≤ 60 percent predicted had significantly reduced normalized diaphragm descent compared to controls. Diaphragm descent ≤ 2 cm per meter height was associated with globally advanced disease progression including poor respiratory function, inability to ambulate, and high levels of lower extremity and abdominal muscle fat infiltration. Interestingly, during maximal expirations, there was also altered diaphragm movement with many individuals having paradoxical diaphragm descent rather than elevation. There is evidence that the diaphragm is active during maximal expiratory efforts and coughing, and one hypothesis for the paradoxical movement is that diaphragm co-contraction may lead to a small degree of diaphragm descent in DMD [32, 33].

AP chest wall expansion and depression during maximal breathing were decreased in DMD, with chest expansion being limited most in the subgroup with MIP ≤ 60 percent
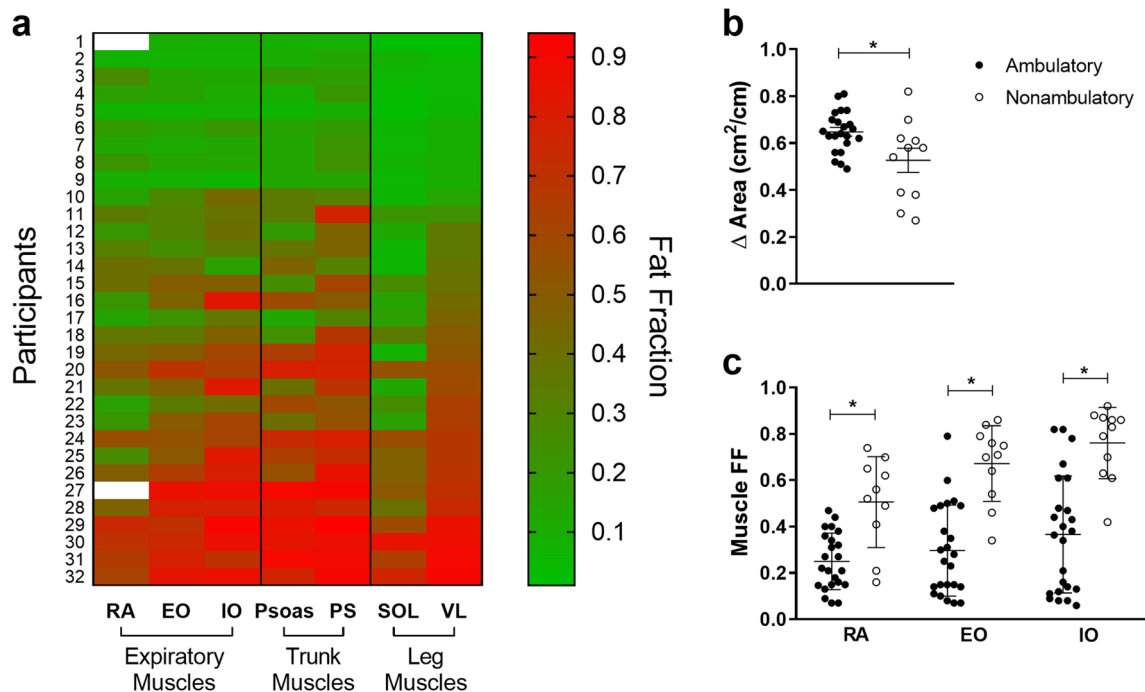
Fig. 6 Respiratory MR biomarkers, LE MR biomarkers, and ambulatory status. **a** To assess the relationship between disease progression in the expiratory muscles and other skeletal muscles, expiratory muscle FF, lower trunk muscle (psoas and PS) FF, and lower extremity muscle (VL and SOL) FF were compared. White cells represent missing data. The relationship between FF of the different muscles was generally consistent with lower fatty infiltration of the expiratory muscles being associated with lower fatty infiltration of the trunk and lower extremity muscles. However, some individuals stand out as having one muscle which is more severely affected than the others. For example, participant 11 has a higher paraspinal FF than would be expected given the FF in his other muscles, and participant 16 has a higher IO FF than may be expected. **b** During maximal inspirations, nonambulatory individuals had significantly smaller increases in sagittal lung area normalized to height, compared to ambulatory individuals ($p = 0.046$). **c** Nonambulatory participants also had significantly higher expiratory muscle FF compared to ambulatory participants ($p < 0.001$ for all comparisons). (*EO* external oblique, *FF* fat fraction, *IO* internal oblique, *PS* paraspinals, *RA* rectus abdominis, *SOL* soleus, *VL* vastus lateralis)

predicted. For chest depression, there was no significant relationship between chest wall movement and age or clinical measures of respiratory function. Mankodi et al. also found decreased chest wall movement in participants with DMD; however, in that study, movement area was assessed rather than movement length, which could be confounded by thoracic cavity size and stature [24]. Although muscle weakness is a primary factor impacting chest wall mobility, particularly during forced expirations, future studies should investigate other possible contributing factors including costovertebral joint stiffness, scoliosis, altered rib cage biomechanics, and body habitus.

MR assessment of muscle fatty infiltration has become a popular tool to determine patterns of muscle involvement and quantify disease progression in DMD [17], yet prior to this investigation, there have been no published results investigating fatty infiltration of the respiratory muscles. This study utilized CSE MRI to assess fatty infiltration in the primary muscles of forced expiration, including the rectus abdominis, external oblique, and internal oblique, as well as the intercostals, which are accessory respiratory muscles

involved in quiet inspiration and maximal breathing. Of the expiratory muscles, the internal oblique tended to show the earliest signs of involvement, reaching FF values > 0.50 even in ambulatory individuals, and the rectus abdominis was consistently the least affected of the expiratory muscles. Fatty infiltration of the expiratory muscles was reflected functionally as decreased MEPs, and in some cases, elevated FF was even present prior to decreases in %pMEP. Interestingly, FF of the IO, EO, and RA was not correlated to peak cough flow or chest depression during forced exhalations.

One unexpected finding from CSE MRI of the chest was the relatively limited fatty infiltration of the intercostal muscles. Although the intercostals were too small to evaluate quantitatively, visual assessment of high resolution CSE images in the coronal and axial plane revealed limited fatty infiltration of these muscles even in many participants with nearly complete fatty replacement of other muscles surrounding the ribcage (Fig. 4). Fatty replacement was only appreciably visible in one individual requiring BiPAP and daytime NIV (FVC = 0.79 L, MIP = 37%, MEP = 36%). The observed relative sparing of the intercostal muscles has not

been reported in the DMD literature before. In one older study that performed external intercostal muscle biopsies, histology of the muscle demonstrated degenerative changes consistent with those seen in limb muscle in a steroid untreated 9 year old participant [34]. However, in the present study, the intercostals visually appeared to be much less infiltrated with fat in comparison to other chest muscles, though we acknowledge that there may be other dystrophic changes taking place that are not captured by CSE MRI.

CSE imaging of the chest also revealed the progressive change in composition of the tissue surrounding the rib cage. In unaffected controls, healthy muscle tissue surrounds the rib cage, whereas in DMD, as muscle degeneration occurs, the ribcage becomes surrounded by fibrofatty tissue. In the majority of nonambulatory participants in this study, the chest wall muscles were nearly completely infiltrated with fat. Limb muscle stiffness, assessed by ultrasound shear wave elastography, has been reported to be increased in DMD [35], but stiffness of chest wall muscles has not been assessed. It is not known how replacement of the chest muscles by fibrofatty tissue affects ribcage compliance, rib cage expansibility (including the reduced AP chest motion observed in this study), and overall respiratory function [36].

Dynamic and CSE MRI of the chest and abdomen are not without limitations. One limitation of the study is the time–cost associated with manual analysis of dynamic imaging. Automated processes for dynamic MRI analysis have been developed, and future studies should consider implementing or developing similar software [24, 25]. Another challenge of the study was optimizing the CSE MRI scan parameters. The decision was made to use only free-breathing CSE scans as breath holds can be challenging for some individuals with DMD. With the respiratory gating, as well as the high resolution and large fields of view of the chest, scan time became a limiting factor. Although parallel imaging using SENSE acceleration was utilized to reduce scan time, this can result in higher image noise. Additionally, in the abdominal images used to quantify FF, a short TR time was chosen to decrease scan time; however, at a conservative flip angle of 10°, some amount of T_1 bias was likely present in the images, artificially increasing FF estimates. Attempts to decrease T_1 bias by decreasing the flip angle to 3° led to an unacceptable reduction in signal-to-noise ratio, thus a compromise was made. Despite these limitations, acquisition of high-quality dynamic and CSE imaging was certainly feasible in this cohort, providing a noninvasive method to assess respiratory parameters in vivo. Future studies should also investigate the value of longitudinal studies of respiratory MR biomarkers and consider taking advantage of emerging advances in image acceleration to shorten scan times [37].

In conclusion, this MRI investigation of diaphragm dynamics, chest wall dynamics, and accessory respiratory muscle fatty infiltration has led to new insights into the disease-related changes that contribute to declining clinical respiratory function. Differences in MR measures between controls and individuals with DMD highlight several factors impairing function in DMD such as reduced thoracic cage and diaphragm mobility as well as progressive fatty infiltration of the muscles of forced expiration. Respiratory MR biomarkers may be beneficial as complements to clinical assessments to improve early detection of accessory muscle involvement and to better quantify disease progression of the individual components of the ventilatory pump. These methods may also be easily translated to other neuromuscular disorders.

Compliance with ethical standards

References

1. Mendell JR, Shilling C, Leslie ND et al (2012) Evidence-based path to newborn screening for Duchenne muscular dystrophy. Ann Neurol 71:304–313. https://doi.org/10.1002/ana.23528
2. Moat SJ, Bradley DM, Salmon R et al (2013) Newborn bloodspot screening for Duchenne muscular dystrophy: 21 years experience in Wales (UK). Eur J Hum Genet 21:1049
3. Hoffman EP, Brown RH Jr, Kunkel LM (1987) Dystrophin: the protein product of the Duchenne muscular dystrophy locus. Cell 51:919–928. https://doi.org/10.1016/0092-8674(87)90579-4
4. Peverelli L, Testolin S, Villa L et al (2015) Histologic muscular history in steroid-treated and untreated patients with Duchenne dystrophy. Neurology 85:1886–1893

5. Petrof BJ, Shrager JB, Stedman HH et al (1993) Dystrophin protects the sarcolemma from stresses developed during muscle contraction. Proc Natl Acad Sci 90:3710–3714

6. LoMauro A, Romei M, Gandossini S et al (2018) Evolution of respiratory function in Duchenne muscular dystrophy from childhood to adulthood. Eur Respir J 51:1701418

7. McDonald CM, Meier T, Voit T et al (2016) Idebenone reduces respiratory complications in patients with Duchenne muscular dystrophy. Neuromuscul Disord 26:473–480. https://doi.org/10.1016/j.nmd.2016.05.008

8. Finder J, Mayer OH, Sheehan D et al (2017) Pulmonary endpoints in Duchenne muscular dystrophy. A workshop summary. Am J Respir Crit Care Med 196:512–519. https://doi.org/10.1164/rccm.201703-0507WS

9. Henricson EK, Abresch RT, Cnaan A et al (2013) The Cooperative International Neuromuscular Research Group Duchenne Natural History Study: glucocorticoid treatment preserves clinically meaningful functional milestones and reduces rate of disease progression as measured by manual muscle testing and other commonly used clinical trial outcome measures. Muscle Nerve 48:55–67. https://doi.org/10.1002/mus.23808

10. Hahn A, Bach JR, Delaubier A et al (1997) Clinical implications of maximal respiratory pressure determinations for individuals with Duchenne muscular dystrophy. Arch Phys Med Rehabil 78:1–6

11. Khirani S, Ramirez A, Aubertin G et al (2014) Respiratory muscle decline in Duchenne muscular dystrophy. Pediatr Pulmonol 49:473–481. https://doi.org/10.1002/ppul.22847

12. Mayer OH, Finkel RS, Rummey C et al (2015) Characterization of pulmonary function in Duchenne muscular dystrophy: pulmonary function in DMD. Pediatr Pulmonol 50:487–494. https://doi.org/10.1002/ppul.23172

13. Carlier PG, Marty B, Scheidegger O et al (2016) Skeletal muscle quantitative nuclear magnetic resonance imaging and spectroscopy as an outcome measure for clinical trials. J Neuromuscul Dis 3:1–28. https://doi.org/10.3233/JND-160145

14. Gaeta M, Scribano E, Mileto A et al (2011) Muscle fat fraction in neuromuscular disorders: dual-echo dual-flip-angle spoiled gradient-recalled MR imaging technique for quantification—a feasibility study. Radiology 259:487–494. https://doi.org/10.1148/radiol.10101108

15. Arpan I, Forbes SC, Lott DJ et al (2013) T2 mapping provides multiple approaches for the characterization of muscle involvement in neuromuscular diseases: a cross-sectional study of lower leg muscles in 5–15-year-old boys with Duchenne muscular dystrophy. NMR Biomed 26:320–328. https://doi.org/10.1002/nbm.2851

16. Vohra RS, Lott D, Mathur S et al (2015) Magnetic resonance assessment of hypertrophic and pseudo-hypertrophic changes in lower leg muscles of boys with Duchenne muscular dystrophy and their relationship to functional measurements. PLoS ONE 10:e0128915. https://doi.org/10.1371/journal.pone.0128915

17. Burakiewicz J, Sinclair CDJ, Fischer D et al (2017) Quantifying fat replacement of muscle by quantitative MRI in muscular dystrophy. J Neurol 264:2053–2067. https://doi.org/10.1007/s00415-017-8547-3

18. Bonati U, Hafner P, Schädelin S et al (2015) Quantitative muscle MRI: A powerful surrogate outcome measure in Duchenne muscular dystrophy. Neuromuscul Disord 25:679–685. https://doi.org/10.1016/j.nmd.2015.05.006

19. Barnard AM, Willcocks RJ, Finanger EL et al (2018) Skeletal muscle magnetic resonance biomarkers correlate with function and sentinel events in Duchenne muscular dystrophy. PLoS ONE 13:e0194283

20. Ricotti V, Evans MR, Sinclair CD et al (2016) Upper limb evaluation in Duchenne muscular dystrophy: fat-water quantification by MRI, muscle force and function define endpoints for clinical trials. PLoS ONE 11:e0162542

21. Bruin PFD, Ueki J, Bush A et al (1997) Diaphragm thickness and inspiratory strength in patients with Duchenne muscular dystrophy. Thorax 52:472–475. https://doi.org/10.1136/thx.52.5.472

22. Laviola M, Priori R, D'Angelo MG, Aliverti A (2018) Assessment of diaphragmatic thickness by ultrasonography in Duchenne muscular dystrophy (DMD) patients. PLoS ONE 13:e0200582

23. Kondo T, Kobayashi I, Taguchi Y et al (2000) A dynamic analysis of chest wall motions with MRI in healthy young subjects. Respirology 5:19–25

24. Mankodi A, Kovacs W, Norato G et al (2017) Respiratory magnetic resonance imaging biomarkers in Duchenne muscular dystrophy. Ann Clin Transl Neurol 4:655–662. https://doi.org/10.1002/acn3.440

25. Bishop CA, Ricotti V, Sinclair CDJ et al (2018) Semi-automated analysis of diaphragmatic motion with dynamic magnetic resonance imaging in healthy controls and non-ambulant subjects with Duchenne muscular dystrophy. Front Neurol. https://doi.org/10.3389/fneur.2018.00009

26. Quanjer PH, Stanojevic S, Cole TJ et al (2012) Multi-ethnic reference values for spirometry for the 3–95-yr age range: the global lung function 2012 equations. Eur Respir J 40:1324–1343. https://doi.org/10.1183/09031936.00080312

27. Wilson SH, Cooke NT, Edwards RH, Spiro SG (1984) Predicted normal values for maximal respiratory pressures in Caucasian adults and children. Thorax 39:535–538

28. Triplett WT, Baligand C, Forbes SC et al (2014) Chemical shift-based MRI to measure fat fractions in dystrophic skeletal muscle: MR measurements of fat fraction in dystrophic muscles. Magn Reson Med 72:8–19. https://doi.org/10.1002/mrm.24917

29. Hollin IL, Peay H, Fischer R et al (2018) Engaging patients and caregivers in prioritizing symptoms impacting quality of life for Duchenne and Becker muscular dystrophy. Qual Life Res Int J Qual Life Asp Treat Care Rehabil 27:2261–2273. https://doi.org/10.1007/s11136-018-1891-7

30. Harlaar L, Ciet P, van der Ploeg AT et al (2018) Imaging of respiratory muscles in neuromuscular disease: a review. Neuromuscul Disord 28:246–256. https://doi.org/10.1016/j.nmd.2017.11.010

31. Lamb MM, West NA, Ouyang L et al (2016) Corticosteroid treatment and growth patterns in ambulatory males with Duchenne muscular dystrophy. J Pediatr 173:207–213.e3. https://doi.org/10.1016/j.jpeds.2016.02.067

32. Mantilla CB, Seven YB, Zhan W-Z, Sieck GC (2010) Diaphragm motor unit recruitment in rats. Respir Physiol Neurobiol 173:101–106. https://doi.org/10.1016/j.resp.2010.07.001

33. Melissinos CG, Bruce EN, Goldman MD et al (1981) Pattern of diaphragmatic activity during forced expiratory vital capacity. J Appl Physiol 51:1515–1525. https://doi.org/10.1152/jappl.1981.51.6.1515

34. Stern LZ, Payne CM, Gruener R et al (1975) Intercostal muscle biopsy in human neuromuscular disease. Histochemical and electron microscopic studies. J Neurol Neurosurg Psychiatry 38:900–910

35. Lacourpaille L, Gross R, Hug F et al (2017) Effects of Duchenne muscular dystrophy on muscle stiffness and response to electrically-induced muscle contraction: a 12-month follow-up. Neuromuscul Disord 27:214–220. https://doi.org/10.1016/j.nmd.2017.01.001

36. Lo Mauro A, Aliverti A (2016) Physiology of respiratory disturbances in muscular dystrophies. Breathe 12:318–327. https://doi.org/10.1183/20734735.012716

37. Hollingsworth KG, Higgins DM, McCallum M et al (2014) Investigating the quantitative fidelity of prospectively under sampled chemical shift imaging in muscular dystrophy with compressed sensing and parallel imaging reconstruction. Magn Reson Med 72:1610–1619. https://doi.org/10.1002/mrm.25072